URSI GASS 2023, Sapporo, Japan, 19 – 26 August 2023

An Ultra-wideband Feed Horn for the Green Bank Telescope

Steven White* [(1)] Robert Simon[(1)], Jack Nelson[(1)], Galen Watts[(1)], Ryan Lynch [(1)],
Laura Jensen[(4)], Alyssa Bulatek[(2)], Maile Harris[(3)], Scott Ransom[(4)]
(1) Green Bank Observatory, Green Bank, WV; email;swhite@nrao.edu; rsimon@nrao.edu; jneslon@nrao.edu; gwatts@nrao.edu; rlynch@nrao.edu;
(2) University of Florida, Gainesville, FL; abulatek@ufl.edu;
(3) Yale University, Johns Hopkins Applied Physics Laboratory; maile.harris@jhapl.edu;
(4) National Radio Astronomy Observatory, Charlottesville, VA; sransom@nrao.edu; ljenson@nrao.edu

Abstract

An ultra-wideband feed horn is designed and fabricated for the frequency range 0.7 to 4 GHz. The scientific goal is to improve pulsar timing observations characterizing frequency-dependent effects and improving signal to noise using greater bandwidth. Given the GBT optics, mechanical limitations constrained the optimization of maximum aperture efficiency to minimum system noise temperature ratio. To achieve these goals a quad-ridge design is selected. A technique is developed for manufacture of a low loss vacuum window with adequate strength and low permeability. Measurements of the far field patterns, noise temperature, and GBT system equivalent flux density are compared to the model-based predictions. Modifications of the ridge profiles to control the modal content and improve efficiency are explored.

1 Introduction

To improve pulsar timing a dual polarization feed covering the frequency range 0.7 to 4 GHz is designed for the Green Bank Telescope prime focus. Recent developments in quadruple-ridge flare horn (QRFH) designs proved promising and provided impetus for undertaking the design effort [1-3]. Without analytic expressions for electric fields propagating in the feed, a 3d simulation program, CST, provided the reflection coefficient and far field patterns necessary for efficiency and modal content estimates [6]. This design effort reconciles the CST predictions with antenna range fair field measurements and then ultimately GBT system equivalent flux density (SEFD) measurements. With predictions and measurements aligned, the models can be optimized to improve performance to satisfy the science goals. For optimized antenna gain to noise ratio necessary for improved timing, GBT optics dictate an aperture diameter of 900 millimeters making the construction of a cryogenic dewar vacuum window challenging. A material dependent minimum thickness specification that can withstand atmospheric pressure typically distorts the far field patterns. Thus, the window is positioned away from the feed aperture and toward the coaxial to waveguide transition. The smaller diameter reduces both window thickness and the thermal gap. A vacuum forming technique is developed with fused quartz fabric infused with optical grade epoxy. Several techniques are employed to improve the total efficiency, reduce spillover, and minimize the phase center location. A differential amplifier with a 100 Ohm input impedance lowers reflections from the transition to free space impedance. Flaring the width of each ridge and dielectric loading generates the proper modal content to reduce the phase center variation across the frequency band and increase illumination efficiency. A corrugation section is added to reduce spillover at the lower end of the band.

2 Feed Design.

With an offset design, the effective focal to diameter ratio is 0.7 requiring a half angle of 39 degrees, a very high gain feed. Because of size constraints, the feed is located at prime focus where spillover becomes a significant contribution to the system noise budget. Hybrid mode feed horns are limited in bandwidth to ~2:1, thus a QRFH design is investigated to determine if the antenna gain over system temperature ratio would ultimately improve pulsar timing. CST generated far fields analyzed for total aperture efficiency determined that all elements in previous designs were necessary to achieve the specifications for improved pulsar timing. These are a coaxial feed differential amplifier design, an exponential horn and ridge profile, a flared ridge profile, a dielectric element, and corrugations. The length and flare angle of the feed to first order determines the field taper at the edge of the dish. The taper is adjusted to minimize spillover while maintaining sufficient aperture efficiency. The differential amplifier is constructed from a Krytar hybrid followed by a Low Noise Factory LNA. A coupler follows the output of the LNA to allow injection of a noise calibration signal. The lower sections of the feed from the coaxial transition to the end of the ridges are enclosed in a vacuum dewar for cryogenic cooling. The entire feed is wrapped in super insulation with two CTI model 1020 refrigerators providing the heat lift. The waveguide window is constructed from quartz fabric to provide the low loss vacuum seal.

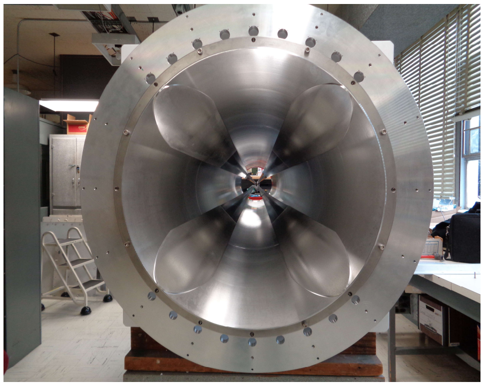

Figure 1. The aperture end view of the feed. The dielectric (1 m x 43 mm spear), warm section of the feed outside the dewar, and corrugated section are not installed. The total length is 1.5 m with 1.2 m inside the dewar. The five corrugations extend the aperture diameter from 0.9 m extended to 1.4 m. The input circular WG diameter is 0.164 m.

3 Window Construction

The section of the feed that is cryogenically cooled requires a large diameter vacuum window. The window must have good RF properties, with minimal permeation in order to provide long-term reliable receiver operation. Traditional closed-cell foams were ruled out due to the thickness that would be required to maintain vacuum integrity during cryogenic operation. After a study of several possible window designs, we settled on developing an epoxy infused hemispherical quartz dome.

Vacuum infusion is often used in applications where high strength and low weight are desired. An added challenge for this project is the need for long-term vacuum integrity. The window is composed of several layers of quartz fabric infused with epoxy. Both the quartz and epoxy are selected based on RF modeling (dielectric properties), and mechanical properties. A hemispherical cap design provides much higher strength when compared to a flat disk. Stress analysis software optimized the design for the minimum dome thickness and height that achieved a safety factor of six times the atmospheric pressure load.

The CST model predicts a greater reflection coefficient than measured as shown in Figure 3. The thermal gap necessary to reduce the conductive heat load from the window is predicted to distort the far field and reduce efficiency. Estimating the ratio of epoxy to quartz fabric gives a combined dielectric constant of 3.75. However, VNA measurements indicate that the dielectric constant is closer to 2.5. We surmise the lower value is from voids in the constructed window.

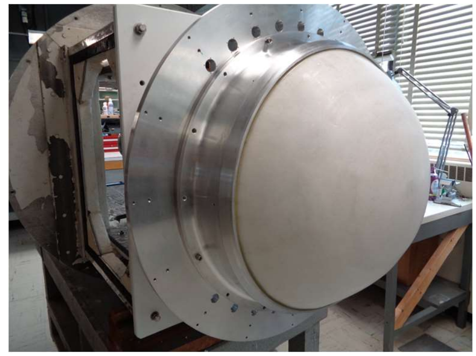

Figure 2. The dome is approximately 610 mm diameter, with a height of 180 mm. The center portion of the dome is 4 mm, and tapers thicker at the rim. Once vacuum infused and the epoxy cured, the dome is bonded into an aluminum ring. The dome/ring assembly is o-ring sealed against the vacuum.

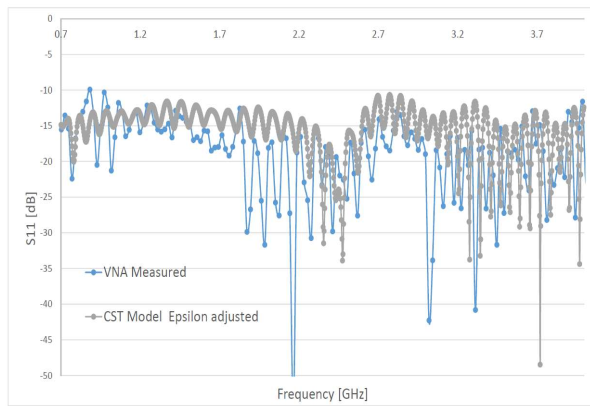

Figure 3. The VNA measured differential reflection coefficient compared to CST model prediction. The CST model dielectric constant for the window is adjusted to 2.5 to match the measured results.

4 Far Fields and Efficiency Analysis

The CST 3D model produces far fields that are exported to calculate illumination, spillover, phase, and cross polarization components for a total aperture efficiency calculation [4]. The spillover prediction is combined with noise contributions from the feed components, differential LNA, CMB, galaxy, and atmosphere to give $\frac{T_{sys}}{\xi_T}$; the parameter that predicts pulsar timing error from the GBT receiver system contribution. The phase efficiency is dependent upon the phase center of the feed for a particular frequency relative to the GBT focal point. For this calculation the CST origin is fixed to the average phase center location across the band. The component contributions for the total efficiency is shown in Figure 4. The total efficiency is given in Figure 5 and compared to the model without the dielectric.

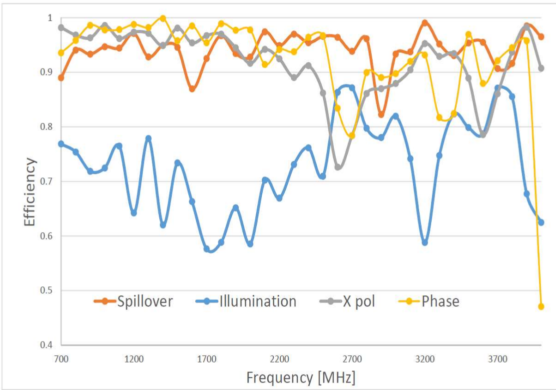

Figure 4. Illumination, spillover, cross polarizaton and phase efficiency are calculated from CST produced far field patterns.

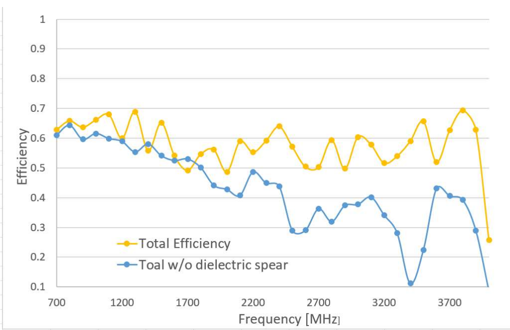

Figure 5. Total efficency comparison calculated from CST produced far field patterns: the yellow curve is with the dielectric, the blue curve is without the dielectric spear.

4 Modal Content

To maintain sufficient aperture efficiency additional modes must be excited as described by Ludwig [5]. Without analytic solutions for the modal content, adjusting the structure of the feed elements to excite desired modes along the length of the feed is difficult. The optimal modal contribution is unknown; however, analysis does provide insight on the far field pattern and ultimately efficiency calculations. Figure 6 shows the asymmetric high order modes TE31 and TM31 content that reduces cross polarization and phase efficiency.

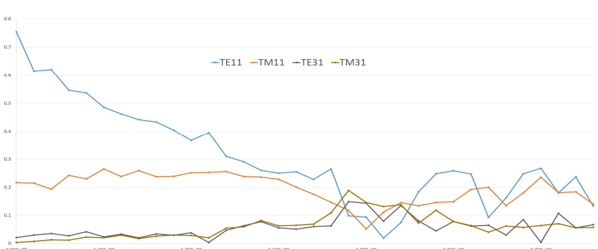

Figure 6. Normalized modal content for modes TE11, TM11, TE31,TM31.

5 Measurements

After construction the feed was installed on an antenna range and measured. The measurement was conducted with all the parts but the LNA and was not cryogenically cooled. The D plane patterns are shown in Figure 7.

With the feed consturcted and software written, the receiver was installed on the GBT for commissioning. By observing the flux of a known calibrator, the SEFD can be calculated and comparted to the predicted values for $\frac{T_{sys}}{\xi_T}$ shown in Figure 8. The values are scaled based on the known GBT aperture size.

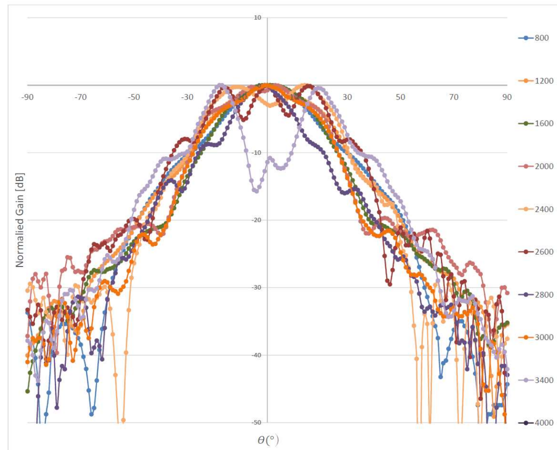

Figure 7. Measured D plane (45˚) far field measurements for select frequencies. The patterns are normalized and in dB.

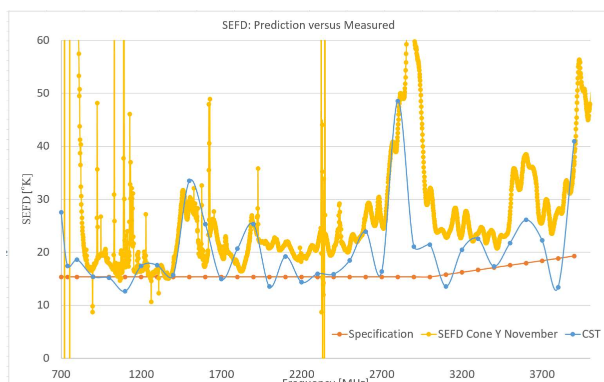

Figure 8. Total System Temperature over efficieny plot converted to same scale as SEFD. The orange curve is the target value for this feed. The yellow curve is the observation determined value from a known flux calibrator (3C295).

6 Improvements

With confidence in the predicted performance versus measured performance, model improvements are explored. The ridge and horn profile are optimized using the exponential and linear component equation (1) with variables: input WG radius a_{yi}, aperture radius a_{yo},, linear component A, exponential profile p, and length L. The ridge width, r_x, is determined by the exponent equation (2) with r_{xmax} the width at the thermal gap. The simplification is necessary to ensure machinability given the large dimensions.

$$a_y(z) = a_{yi} + (a_{yo} - a_{yi})((1-A)\frac{z}{L} + A\left(\frac{z}{L}\right)^p) \quad (1)$$

$$r_x(z) = r_{xmax} + r_{xmax} * \left(1 - e^{-\left(\frac{z}{L}\right)^2}\right) \quad (2)$$

$$a_y(z) = A * (c_1 e^{rt} + c_2) + (1-A)(a_{yi} + (a_{yo} - a_{yi})\frac{z}{L}) \quad (3)$$

$$c_1 = \frac{(a_{yo} - a_{yi})}{e^{pL} - 1} \quad (4)$$

$$c_2 = \frac{(a_{yi}\, e^{pL} - a_{yo})}{e^{pL} - 1} \quad (5)$$

With machining experience the possibility of a more complex ridge profile is explored. An optimization with equations (3-5) allows control of the flare angle in the symmetry plane. [1] Analysis of the FF modal content shows a reduction in the asymmetric azimuthal modes and increased efficiency. Also, there appears to be larger than predicted noise contribution from one of the feed components, possibly the coaxial to ridge transition. Additional measurements are forthcoming to separate excess thermal noise contribution from efficiency and validate the calibration injection values. A design to reduce the loss and lower the cryogenic temperature could possibly improve the total noise temperature at the upper portion of the band. Figure 9 illustrates the results from optimization of the ridge profile. Figure 10 gives the modal content and can be compared with Figure 6.

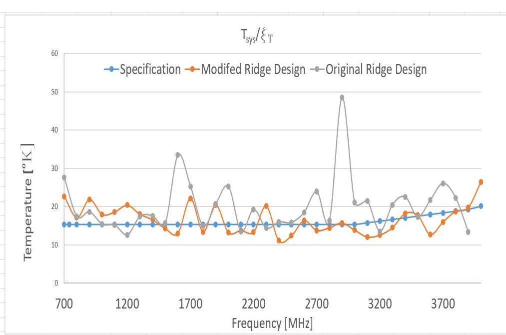

Figure 9. Total System Temperature over efficieny plot converted to same scale as SEFD. The blue curve is the target value for this feed. The slate curve is the as built ridge profile. The orange curve is from the modified ridge profile model.

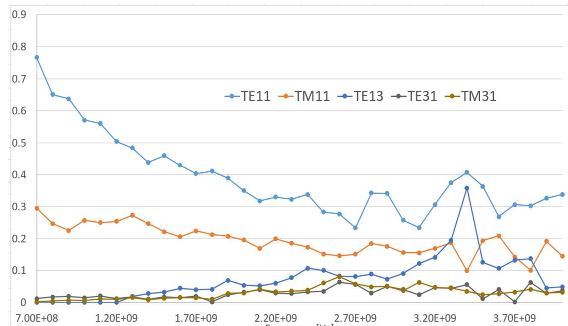

Figure 10. Optimizing the ridge profile increases the modal content for modes TE11 and reduces the TE31 and TM31 content.

Acknowledgements

Dennis Egan, Phillip Doolittle, Mike Hedrick, Roger Dickenson, Harry Sipe, Pat Schaffner and Dwyane Barker manufactured the feed in the GBO machine shop overcoming many challenges in the process. Art Symmes performed a stress analysis for the vacuum window and developed a thermal model for all the cryogenic components. Joe Brandt, Ramon Creager, Paul Marganian, and Nathaniel Sizemore provided all the software necessary for monitor and control, telescope interface, and digital signal processing of the astronomical data.

This research project was funded in part by the Gordon and Betty Moore Foundation through Grant GBMF7576 to Associated Universities, Inc. for the Green Bank Observatory.

References

[1] T. S. Beukman, "Modal_Based Design Techniques for Circular Quadruple_Ridged Flared Horn Antennas," Dissertation March 2015, University of Stellenbosch.

[2] A. Akgiary. "New Technologies Driving Decade-Bandwidth Radio Astronomy: Auad-Ridged Flared Horn&Compound_Semiconductor LNAs". Thesis 2013. California Institute of Technology.

[3] A. Dunning, M. Bowen, B. Bourne, D. Hayman, S.L. Smith. "An Ultra_Wideband Dielectrically Loaded Quad-Ridged Feed Horn for Radio Astronomy". 2Proc IEEE-APS APWC. 5th Edition. Sept. 2015.

[4] P.-S. Kildal, "Factorization of the feed efficiency of paraboloids and Cassegrain antennas," IEEE Trans. Antennas Propag. Vol. 33, no. 8, pp. 903-908, August 1985.

[5] A.C. Ludwig, "Radiation pattern synthesis for circular aperture horn antennas," IEEE Trans. Antennas Propag. Vol. 14, no.4, pp 434-440, July 1966.

[6] Simulia CST Microwave Studio 2022. Darmstadt. Germany